

Chapter 1

Introduction

1.1 Mott Transition

The band theory of solids had been highly successful in describing metals, insulators, and their transitions. The basic distinction between metals and insulators, based on the band structure, was established in the early years of quantum mechanics, and the derived principles well explained material characteristics including the electronic and optical properties. In 1937, however, several simple transition-metal oxides with a partially filled d -electron band were found to be insulators [1], and then importance of the strong Coulomb repulsion between the electrons was pointed out as a source of the eccentric insulating behavior [2]. In subsequent theoretical approaches, N. F. Mott provided an important foundation of how the electron-electron interactions lead to the insulating phase [3], and then this state is called the Mott insulator. Under the strong on-site electron correlation U , the original band would be split into two bands with energy gap of U , and thus the system would be an insulator.

One striking point of the Mott insulator is that drastic electronic state change emerges associated with the insulator-metal (Mott) transition [4]. In the vicinity of the Mott transition, a wide variety of unprecedented phenomena such as high-temperature superconductivity, colossal magnetoresistance, and large thermoelectric effect arises from interplay among charge, spin, and orbital degrees of freedom, as discussed in detail later. While their functional effects should form the significant basis of future oxide electronics, the detailed mechanisms are still under debate. In this thesis, we focus on a couple of transition-metal oxides considered as key materials to solve the pending problems, and investigate their charge dynamics and Mott transition features via spectroscopy.

1.1.1 Insulator-Metal Transition

The discovery of the Mott insulator advanced the ceaseless effort to understand how the Mott insulating state could emerge from a metal with controllable parameters. This phase transition is termed the insulator-metal (Mott) transition, as noted before. The insulating phase and its remnant fluctuation in metals are indeed the most striking and prominent features of the strongly correlated electrons and have long attracted much attention in this research field.

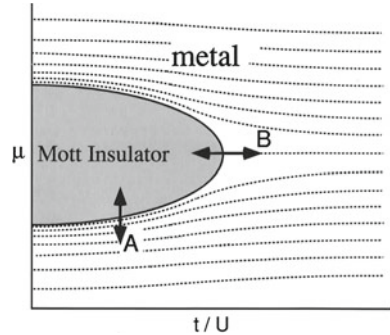
Figure 1.1 illustrates a schematic phase diagram of the Mott insulator and the metal in a plane of μ and t/U . Here μ , t , and U denote the chemical potential, the transfer integral, and the Coulomb correlation, respectively. Dotted curves represent the density contour lines. The Mott transition is of two types, the filling-control type (route A) and the bandwidth-control type (route B). Namely, the filling-control transition has as a control parameter the electron concentration or the band filling n . With doping carriers into the Mott insulating state with integer filling, the system would become a metal. In the bandwidth-control transition, the phase transition would occur with increase of the ratio of the bandwidth to the Coulomb interaction, which enhances the quantum fluctuation and stabilizes the metallic state.

Let us provide a brief explanation of the electronic structure change, taking an example of the bandwidth-control insulator-metal transition. A prototype of theoretical understanding of the correlation effect on the insulator-metal transition was achieved by using the Hubbard model. Its Hamiltonian is given in the following formula.

$$\mathcal{H} = -t \sum_{\langle ij \rangle} (c_{i\sigma}^\dagger c_{j\sigma} + \text{h.c.}) + U \sum_i n_{i\uparrow} n_{i\downarrow} \quad (1.1)$$

Here, $c_{j\sigma}$ and $c_{j\sigma}^\dagger$ are the annihilation and creation operator of electrons at site j , respectively. One of the most important advantages of this model is that the electronic states and the low-energy charge dynamics at low temperatures can be roughly described despite its quite simple formation. J. Hubbard has first

Fig. 1.1 Schematic phase diagram of the Mott transition [4]. Routes A and B represent filling-control type and bandwidth-control type insulator-metal transitions, respectively



theoretically demonstrated the band splitting into upper and lower Hubbard bands under the strong electron correlation and then succeeded in explaining the existence of charge gap in the insulating phase [5]. On the other hand, W. F. Brinkman and T. M. Rice have indicated that the carrier effective mass m^* shows divergent enhancement in the form of $m^*/m \propto (1 - (U/U_c)^2)^{-1}$ in the course of the transition, by applying a Gutzwiller's variational method to the half-filled Hubbard model [6].

One of the notable numerical approaches for applications to real systems is a dynamical mean field theory (DMFT) [7], by which the Hubbard model can be exactly solved in the limit of $d \rightarrow \infty$ (d being the lattice coordination). A solution of the mean field equation shows that the metallic state shows up for $U/t \ll 1$ and the insulating one does for $U/t \gg 1$ at low temperature. By means of the quantum Monte Carlo method, it has been shown that the model has a metal-insulator transition at a value of $(U/t)_c$ assuming the Bethe lattice with the infinite dimension [8]. The calculated density of states variation is shown in Fig. 1.2. The density of states in the insulating phase ($U/t > (U/t)_c$) is characterized by the well separated upper and lower Hubbard bands. On the other hand, the electronic structure near the critical state ($U/t \sim (U/t)_c$) is characterized by the quite narrow quasiparticle band as in the Brinkman-Rice picture as well as the reminiscence of the upper and lower Hubbard bands. When approaching $(U/t)_c$, the central quasiparticle bandwidth becomes narrower with keeping its height. Thus, the one-particle density of states

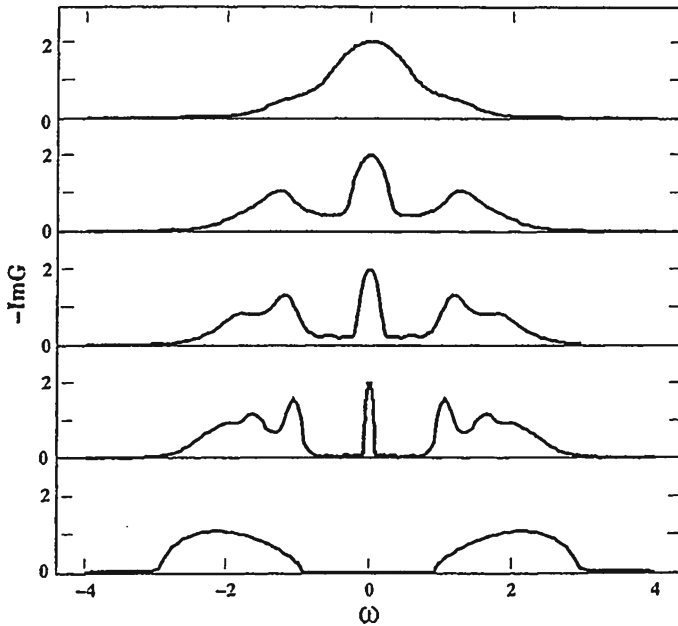


Fig. 1.2 Density of states at zero temperature for the half-filled Hubbard model at $U/2t = 1, 2, 2.5, 3$, and 4 from *top to bottom* [8]

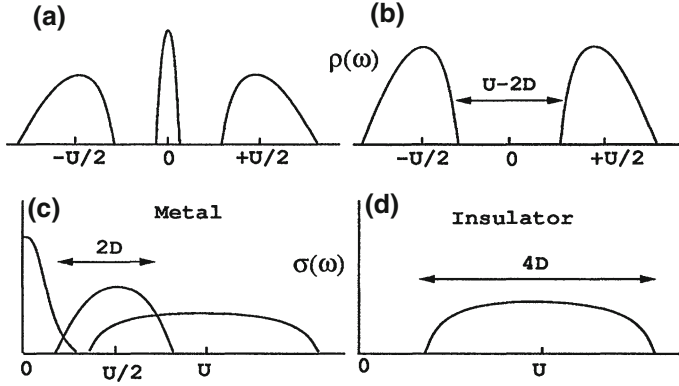


Fig. 1.3 Schematic of the density of states in the **a** metallic and **b** insulating phases [9]. Corresponding optical conductivity spectra in the **c** metallic and **d** insulating states are also shown

discontinuously jumps to the zero value at the Mott transition, giving rise to the discontinuous charge-gap opening.

The optical conductivity spectra expected from this model are schematically illustrated in Fig. 1.3 [9]. In the insulating phase, the band arising from the Mott-gap excitation emerges centered at $\omega = U$. In the metallic phase, on the other hand, there are three peaks, the Drude peak at $\omega = 0$, the incoherent band as originating from the transition between the remaining Hubbard band and the quasiparticle band, and the original Mott-gap excitation. In addition to the discontinuous charge-gap opening, the divergence of the carrier effective mass m^* is expected near the Mott transition. This anomaly can be experimentally observed by measurements of a T -linear term of the electronic specific heat coefficient, susceptibility of the Pauli paramagnetism, inverse of the Drude weight in the optical conductivity spectra, and also a coherent part of the photoemission spectra.

1.1.2 Material Systematics

The Mott insulating state has been first found and studied in a set of simple 3d transition-metal oxides, such as Ti_2O_3 , V_2O_3 , Cr_2O_3 , MnO , FeO , CoO , NiO , and CuO . On the other hand, the Mott-transition behaviors have been investigated mainly in oxides with more controllable parameters [10]. Among a number of ternary and multinary compounds, the most prototypical target material is perovskite oxides such as $R_{1-x}A_x\text{MO}_3$ and $R_{2-x}A_x\text{MO}_4$ (R , A , and M being rare-earth-metal elements, alkaline-earth-metal elements, and 3d transition-metal elements).

As shown in Fig. 1.4, these systems provide a wide-ranging setting for examining the insulator-metal transition. Significance of systematic control of the band filling

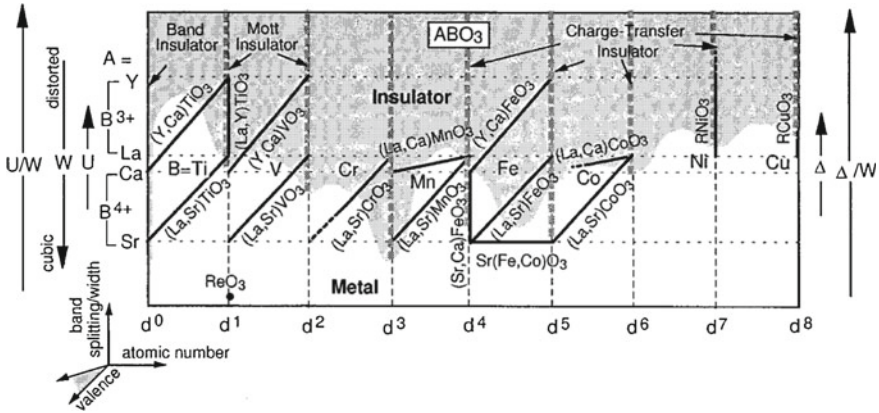


Fig. 1.4 Insulator-metal diagram for the 3d transition-metal perovskite oxides with various controllable parameters [10]

n in correlated oxides has been recognized since the discovery of high-temperature superconductivity in the layered cuprates. In the perovskite oxides and many other compounds, a standard method of the filling control is substitution of the divalent A for the trivalent R sites. The best known examples are $\text{La}_{1-x}\text{Sr}_x\text{TiO}_3$ ($n = 1 - x$) and $\text{La}_{1-x}\text{Sr}_x\text{VO}_3$ ($n = 2 - x$). As for the bandwidth-control Mott transition, the control of the transfer interaction t or the bandwidth W can be easily achieved by modifying the chemical composition through the solid solution or mixed-crystal effect while essentially maintaining the original lattice structure. This type transition is typically observed for RNiO_3 and $\text{V}_{2-x}\text{Ti}_x\text{O}_3$. In the case of RNiO_3 , for example, t/U decreases with the Ni-O network distortion induced by the R ionic size change, and the transition to the Mott insulating phase occurs between $R = \text{La}$ and Pr .

1.1.3 Classification of Charge Gap

The character of low-energy charge excitation or charge gap in the Mott-insulating phase is classified by energy levels of the transition-metal 3d and oxygen 2p bands. The difference between the following two types is schematically illustrated in Figs. 1.5a, b. When the oxygen p level (ε_p) is much lower than the transition-metal d level ε_d , the oxygen p orbital contributes only through virtual processes. This type of transition-metal oxides in which $\varepsilon_d - \varepsilon_p$ is supposed to be larger than U_{dd} is termed a Mott-Hubbard insulator, where the band gap is of the $d-d$ type as in the original Hubbard picture. Because of $U_{dd} < |\varepsilon_d - \varepsilon_p|$, the charge excitation in the Mott-insulating state is dominantly determined by U_{dd} . In contrast, when $|\varepsilon_d - \varepsilon_p|$ is smaller than U_{dd} , the p band is located between the upper and lower Hubbard bands. In this case, the charge gap in the Mott-insulating state is mainly determined

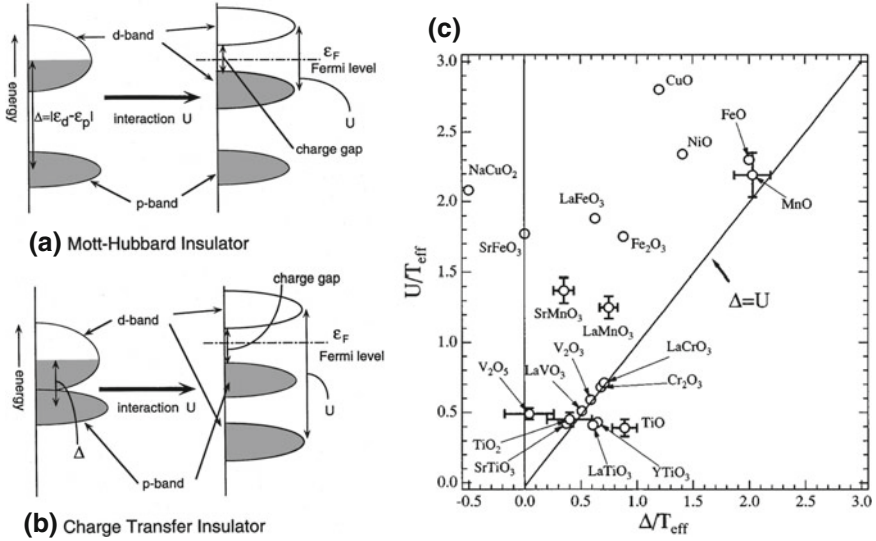


Fig. 1.5 Schematic of energy levels for **a** a Mott-Hubbard insulator and **b** a charge-transfer insulator [4]. **c** Zaanen-Sawatzky-Allen U - Δ plot for 3d transition-metal oxides, deduced from cluster-model analyses of the transition-metal 2p core level photoemission spectra [13]

by the charge transfer type and holes doped into the Mott insulator mainly occupy the oxygen p band. This type of compounds is termed a charge-transfer insulator [11]. The importance of the oxygen band in this class of material has been first pointed out by photoemission and optical spectroscopy in nickel compounds [12].

Figure 1.5c gives the so-called Zaanen-Sawatzky-Allen plot [13], classifying the various transition-metal compounds by the relative magnitudes of the on-site d - d Coulomb energy U and the p - d charge-transfer energy Δ . The straight line for $U = \Delta$ separates the U - Δ diagram into the Mott-Hubbard and charge-transfer regimes. In reality, however, the boundary $U - \Delta$ is not a sharp phase boundary but becomes a crossover region where the charge gap character changes continuously, since the d and p states are mutually hybridized. In general, the late transition-metal compounds such as Cu oxides are characterized by the large Coulomb repulsion energy U and the small charge-transfer energy Δ , and thus are classified as typical charge-transfer compounds. In contrast, the early transition-metal compounds such as Ti and V oxides are characterized by the small U and the large Δ , and thus are classified as typical Mott-Hubbard compounds. These systematics have been experimentally confirmed in M -variation of optical gaps measured for $R_{1-x}A_xMO_3$ [14] and $R_{2-x}A_xMO_4$ [15]. As shown in Fig. 1.5c, on the other hand, the experimental U and Δ values deduced from the analysis of the 2p core-level photoemission spectra [13] suggest that many early transition-metal compounds may be reclassified as intermediate between the charge-transfer regime and the Mott-Hubbard regime.

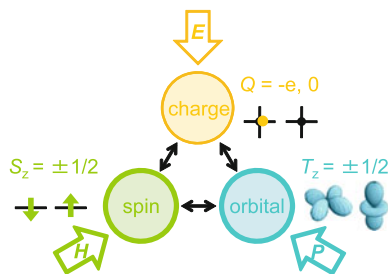
1.2 Charge, Spin, and Orbital Degrees of Freedom

Aside from the control with chemical modification utilizing R and A elements, the $3d$ transition-metal element M has the respective d -electron number ranging from d^1 (Ti^{3+}) to d^9 (Cu^{2+}), and fundamental electronic properties significantly change with the M itself. One main reason is that charge, spin, and orbital degrees of freedom explicitly emerge originating from the strong Coulomb repulsion. The detailed effective degrees of freedom are determined from the d -electron number, the crystal field splitting, and so on. As shown in Fig. 1.6, the various degrees of freedom inherently link to each other, and exhibit large cross-correlation responses to external fields [16]. The motion of the charge gives origin to the electric current and polarization. The spin is an essential factor determining magnetic properties of materials. The orbital represents a shape of the electron cloud in solids, and for example can be a source of anisotropic transport and optical responses.

In the Mott-insulating state of a crystal, the d electrons are almost entirely localized on the respective M sites, which makes the charge, spin, and orbital degrees of freedom combine to produce versatile ordering patterns [17]. Currently the spontaneous order is known to appear in a wide variety of transition metal oxides, such as perovskite manganites [18], ferrites [19], cobaltites [20], nickelates [21, 22], and cuprates [23], and cooperation and competition of the ordering give rise to rich electronic phase diagrams in the correlated oxides. Prototypical cases for quasi-two-dimensional oxides having a single-layered perovskite structure $R_{2-x}A_x\text{MO}_4$ are displayed in Fig. 1.7. In one of the stable phases, the doped holes and spins form stripes running along the diagonal direction in $\text{La}_{2-x}\text{Sr}_x\text{NiO}_4$ ($x = 1/3$) and the horizontal direction in $\text{La}_{2-x}\text{Ba}_x\text{CuO}_4$ ($x = 1/8$). In a half-doped state of $\text{La}_{2-x}\text{Sr}_x\text{MnO}_4$ ($x = 1/2$), a checkerboard-type charge ordering appears associated with a characteristic spin-orbital order pattern running along the zigzag chains.

One striking point is that dramatic changes of magnetic, transport, and also optical properties emerge near the Mott transition, in which the electrons are especially nearly delocalized but mutually correlated while having the above degrees of freedom. A typical example is a colossal magnetoresistance (CMR) effect observed in the perovskite manganites [24]. In the CMR manganites, the drastic decrease in the resistivity is induced by applying the magnetic field, impressing the electric

Fig. 1.6 Coupled response arising from charge, spin, and orbital degrees of freedom



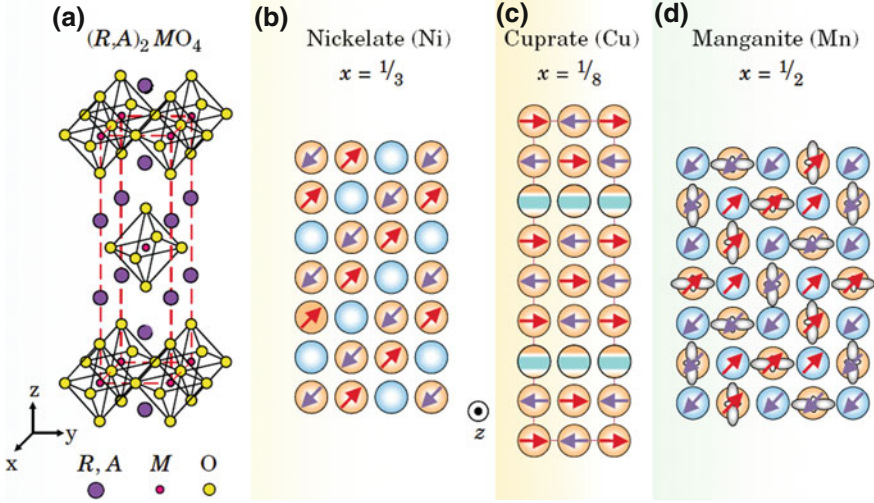


Fig. 1.7 Spontaneous charge-spin-orbital ordering with a wide variety of patterns in layered perovskite oxides $R_{2-x}A_xMO_4$ [17]

voltage, and exposing the light. It is recognized that the rigidly-linked spin and orbital degrees of freedom play an essential role in the CMR effect. Other example of the emergent phenomena is high-temperature superconductivity in the layered cuprates [25]. While charge ordering usually causes the electrical insulation, in the cuprates the conduction can persist along the stripe direction because of its partial filling in the stripes (Fig. 1.7c). Although the relationship between the metallic stripes and the high-temperature superconductivity remains under debate, the discovery of the stripe order undoubtedly indicates the existence of many other electronic phases competing on the CuO_2 plane.

1.3 Fundamental Spectroscopic Results

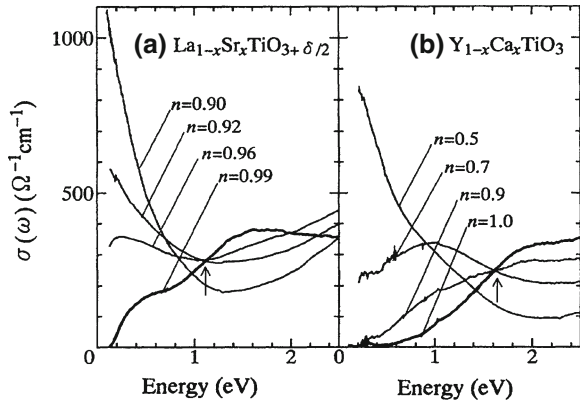
As noted in the above section, the several degrees of freedom of the correlated electrons present more complex faces of the insulator-metal transition, and their coupling produces the various intriguing phenomena in the vicinity of the transition. In the context of the burgeoning research field, spectroscopic study has been a powerful probe for investigating the electronic structure change in the diverse phenomena, and indeed has achieved significant results. The previously obtained data cover a lot of ground and we have no intention of going into all the details here. In this section, we briefly overview some fundamental and important features of the charge dynamics observed near the Mott transition, while the further introduction and the problem presentation are described in the respective chapters.

1.3.1 Mott-Scale Reconstruction

One characteristic feature in the typical Mott transitions of the correlated d -electron oxides is that the Mott gap collapses with the temperature change or the chemical doping as a result of the reconstruction of the electronic structure on a large energy scale comparable to the Coulomb repulsion (\sim several eV) upon the insulator-metal transition. In Fig. 1.8 we show the optical conductivity spectra evolution in the typical filling-control Mott-transition system perovskite titanates [26]. While the Mott-gap structure is clearly observed in the insulating phase, the spectral weight transfer occurs on the Mott scale with increasing the doped holes, and finally the structure evolves into the large Drude peak.

This Mott-scale electronic structure reconstruction is universally observed in many other Mott-transition oxides even including the colossal magnetoresistive manganites and the high-temperature superconducting cuprates. Fig. 1.9 gives the temperature and doping variation of the optical conductivity spectra in (a) $\text{La}_{1-x}\text{Sr}_x\text{MnO}$ [27] and (b) $\text{La}_{2-x}\text{Sr}_x\text{CuO}$ [28]. With change of the temperature or the doping level, the electronic structure varies in a similar wide energy scale. On the other hand, further information can be obtained from analysis of the detailed additional feature. In $\text{La}_{1-x}\text{Sr}_x\text{MnO}$, for example, unconventional temperature dependence with an interband-like transition has been ascribed to the electronic structure change of the e_g electrons with the spin polarization [27]. In the case of $\text{La}_{2-x}\text{Sr}_x\text{CuO}$, pseudogap formation is clearly confirmed in the mid-gap state, and relationship to other factors such as some sort of fluctuation, preformed singlet pairs, and potential resonating valence bond state has been discussed. Such a spectral weight transfer has been studied also by the photoemission spectroscopy.

Fig. 1.8 Typical example of optical conductivity spectra variation in the Mott transition, measured in $\text{La}_{1-x}\text{Sr}_x\text{TiO}_{3+\delta/2}$ and $\text{Y}_{1-x}\text{Ca}_x\text{TiO}_3$ [26]. Electronic structure reconstruction on a large energy scale can be observed



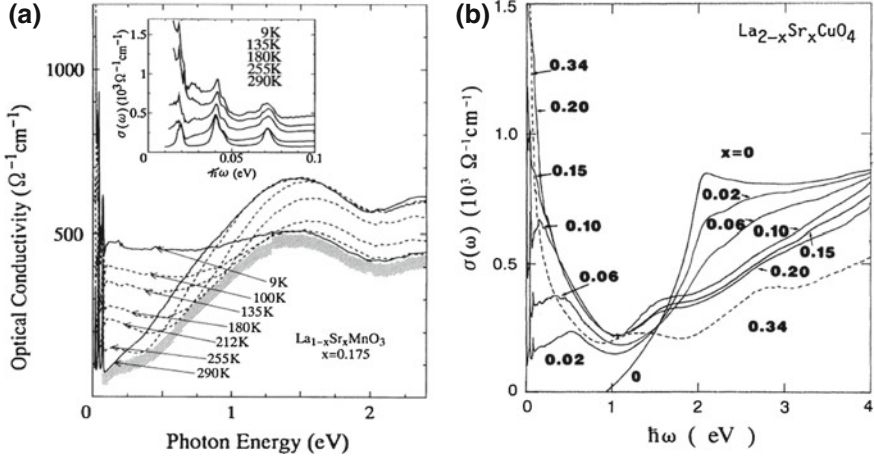


Fig. 1.9 Optical conductivity spectra evolution in **a** colossal magnetoresistive manganite $\text{La}_{1-x}\text{Sr}_x\text{MnO}_3$ ($x = 0.175$) [27] and **b** high-temperature superconducting cuprate $\text{La}_{2-x}\text{Sr}_x\text{CuO}_4$ ($x = 0 - 0.34$) [28]

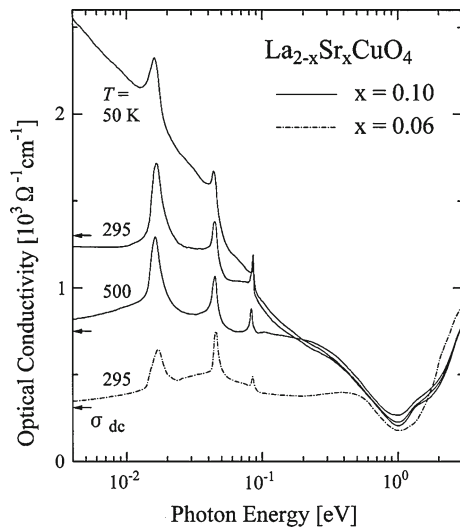
1.3.2 Incoherent Carrier Dynamics

Strong incoherence in the metallic state has also recognized to be one common property of the most transition-metal oxides near the Mott-transition point. The incoherent carrier dynamics as well as other anomalies in charge, spin, and orbital fluctuations arise from almost localized but barely itinerant electrons in the metallic region proximate to the Mott-insulating phase. As one example, we take the rather energy-flat feature of the optical conductivity spectra as observed in the incoherent metal. In Fig. 1.10, we show the temperature variation of the in-plane optical conductivity of lightly-doped $\text{La}_{2-x}\text{Sr}_x\text{CuO}_4$ [29], which typically shows the absence of resistivity saturation at the Mott limit. With increasing the temperature, the Drude peak easily collapses into a broad structure with maximum around several tens meV. This feature is typical of the incoherent metal, and widely observed in many other systems from rather low temperatures near the Mott critical region. The incoherent carrier dynamics has been also investigated based on the photoemission spectra.

1.3.3 Momentum Variation

It is worth noting also the momentum dependence of the charge dynamics near the Mott transition. This point has been intensively studied by angle-resolved photoemission spectroscopy in the superconducting cuprates. Aside from the d -wave superconducting gap, a pseudogap opens with the same momentum-space symmetry as the superconducting gap [30]. This partially gapped Fermi surface is termed

Fig. 1.10 In-plane optical conductivity of $\text{La}_{2-x}\text{Sr}_x\text{CuO}_4$ ($x = 0.06$ – 0.10) [29]. Arrows indicate dc conductivity calculated from the in-plane resistivity



Fermi arc, which is believed to be a hallmark of the high-temperature superconductors. However, the issue what kind of order or fluctuation dominates the pseudogap state is still under debate. Fig. 1.11 shows momentum distribution of the spectral weight at E_F for slightly-doped $\text{La}_{2-x}\text{Sr}_x\text{CuO}_4$ [31]. A quasiparticle peak crosses the Fermi level only around the nodal direction of the d -wave superconducting gap, forming the Fermi arc. The $(\pi, 0)$ antinodal spectra show the pseudo-gapped behavior and its structure gradually evolves with approaching the Mott insulating state. On the other hand, similar study in other Mott-transition oxides has scarcely been conducted

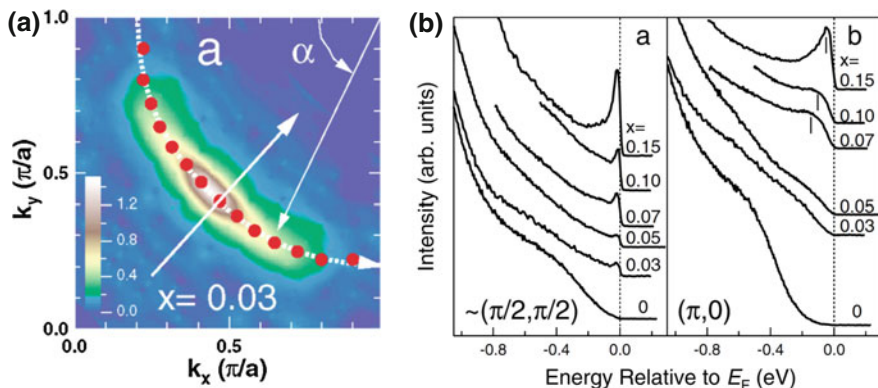


Fig. 1.11 **a** Spectral weight at the Fermi energy for $\text{La}_{2-x}\text{Sr}_x\text{CuO}_4$ ($x = 0.03$) plotted in the momentum space. **b** Doping variation of energy distribution curves at the Fermi wavenumber in the nodal and antinodal directions [31]

yet, and it is not clear whether this momentum-dependent feature is inherent in the proximity to the superconducting or the Mott-insulating state.

1.4 Purpose of this Thesis

The spectroscopic study is highly effective for investigating the complicated electronic structure change in charge-spin-orbital coupled phenomena of the Mott-transition oxides, as introduced in the last section. On the other hand, the detailed mechanisms in specific phenomena and the roles of the respective degrees of freedom remain to be completely elucidated. In this thesis, we aim to reveal the carrier dynamics commonalities and/or differences underlying the emergent phenomena and extend the Mott-physics appropriately. For this purpose, we adopt several counterpart transition-metal oxides (Fig. 1.12) as model systems suitable for examining the mechanisms, and investigate their detailed electronic structures via spectroscopy.

In Chap. 3, we examine the high-temperature carrier dynamics and thermoelectric response in a typical filling-control Mott transition system $\text{La}_{1-x}\text{Sr}_x\text{VO}_3$. In the vicinity of the Mott transition, it is expected that incoherent carrier dynamics appears with increasing temperature and the thermopower undergoes crossovers, asymptotically approaching the limit values expected from the entropy consideration.

In Chap. 4, we take up a doped valence-bond solid system $(\text{Ti}_{1-x}\text{V}_x)_2\text{O}_3$, especially with the focus on the eccentric insulator-metal transitions. Charge dynamics in thermally and doping induced insulator-metal transitions is examined by systematically measuring the transport and optical properties. In addition, we further closely examine the dynamics of the doped holes, including a highly doped metallic region.

In Chap. 5, we systematically investigate charge dynamics and electronic structures for layered nickelates $\text{R}_{2-x}\text{Sr}_x\text{NiO}_4$, an important counterpart to the isostructural

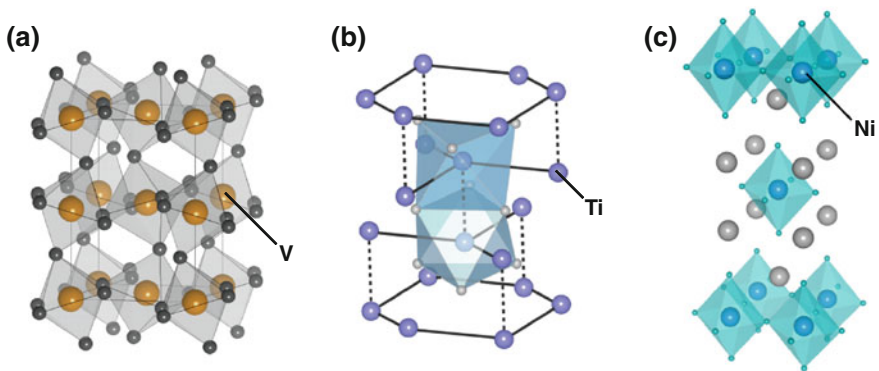


Fig. 1.12 Target materials in this thesis. **a** $\text{La}_{1-x}\text{Sr}_x\text{VO}_3$, **b** $(\text{Ti}_{1-x}\text{V}_x)_2\text{O}_3$, and **c** $\text{R}_{2-x}\text{Sr}_x\text{NiO}_4$

superconducting cuprate $\text{La}_{2-x}\text{Sr}_x\text{CuO}_4$. We perform high-resolution laser angle-resolved photoemission spectroscopy on the barely-metallic nickelate for revealing the Fermi surface and the momentum-resolved charge dynamics to be compared to the superconducting cuprates. In the metallic state with charge-ordering instability, pseudogap-related charge dynamics and anomalous transport properties distinguished from the Fermi liquid behaviors are also expected to be observed. In addition, we examine the electronic structure evolution including the orbital character. For clarifying orbital-resolved three-dimensional Fermi surface structures in this nickelate system, we perform energy-dependent soft-x-ray angle-resolved photoemission spectroscopy. The doping variation of the hole orbital states is also investigated by soft-x-ray absorption spectroscopy.

In Chap. 6, finally, we conclude this thesis with summarizing the main results.

References

1. de Boer JH, Verwey EJW (1937) Proc Phys Soc 49:59
2. Mott NF, Peierls R (1937) Proc Phys Soc 49:72
3. Mott NF (1937) Proc Phys Soc A 62:416
4. Imada M, Fujimori A, Tokura Y (1998) Rev Mod Phys 70:1039
5. Hubbard J (1964) Proc R Soc London A 281:401
6. Brinkman WF, Rice TM (1970) Phys Rev B 2:4302
7. Georges A, Kotliar G, Krauth W, Rozenberg MJ (1996) Rev Mod Phys 68:13
8. Zhang XY, Rozenberg MJ, Kotliar G (1993) Phys Rev Lett 70:1666
9. Rozenberg MJ, Kotliar G, Kajueter H, Thomas GA, Rapkine DH, Honig JM, Metcalf P (1995) Phys Rev Lett 75:105
10. Fujimori A (1992) J Phys Chem Solids 53:1595
11. Zaanen J, Sawatzky GA, Allen JW (1985) Phys Rev Lett 55:418
12. Fujimori A, Minami F (1984) Phys Rev B 30:957
13. Bocquet AE, Mizokawa T, Morikawa K, Fujimori A, Barman SR, Maiti K, Sarma DD, Tokura Y, Onoda Phys M (1996) Rev B 53:1161
14. Arima T, Tokura Y, Torrance JB (1993) Phys Rev B 48:17006
15. Matsuno J, Okimoto Y, Kawasaki M, Tokura Y (2005) Phys Rev Lett 95:176404
16. Tokura Y, Nagaosa N (2000) Science 288:462
17. Tokura Y (2003) Phys Today 56:50
18. Jirak Z, Krupicka S, Simsa Z, Dlouha M, Vratislav S (1985) J Magn Magn Mater 53:153
19. Takano M, Takeda Y, (1983) Bull Inst Chem Res. Kyoto Univ. 61:406
20. Zalitznyak IA, Hill JP, Tranquada JM, Erwin R, Moritomo Y (2000) Phys Rev Lett 85:4353
21. Chen CH, Cheong S-W, Cooper AS (1993) Phys Rev Lett 71:2461
22. Kajimoto R, Ishizaka K, Yoshizawa H, Tokura Y (2003) Phys Rev B 67:014511
23. Tranquada JM, Sternlieb BJ, Axe JD, Nakamura Y, Uchida S (1995) Nature 375:561
24. Tokura Y (2006) Rep Prog Phys 69:797
25. Ginzburg DM (1992) Physical Properties of High Temperature Superconductors, vol 3. World Scientific, Singapore
26. Okimoto Y, Katsufuji T, Okada Y, Arima T, Tokura Y (1995) Phys Rev B 51:9581
27. Okimoto Y, Katsufuji T, Ishikawa T, Urushibara A, Arima T, Tokura Y (1995) Phys Rev Lett 75:109
28. Uchida S, Ido T, Takagi H, Arima T, Tokura Y, Tajima S (1991) Phys Rev B 43:7942
29. Takenaka K, Shiozaki R, Okuyama S, Nohara J, Osuka A, Takayanagi Y, Sugai S (2002) Phys Rev B 65:092405

30. Damascelli A, Hussain Z, Shen Z-X (2003) Rev Mod Phys 75:473
31. Yoshida T, Zhou XJ, Sasagawa T, Yang WL, Bogdanov PV, Lanzara A, Hussain Z, Mizokawa T, Fujimori A, Eisaki H, Shen Z-X, Kakeshita T, Uchida S (2003) Phys Rev Lett 91:027001

Spectroscopic Study on Charge-Spin-Orbital Coupled
Phenomena in Mott-Transition Oxides

Uchida, M.

2013, XII, 103 p., Hardcover

ISBN: 978-4-431-54296-4